JOURNAL OF MATERIALS SCIENCE **36** (2001) 67–75

Reaction of magnesium boride particles in mechanically alloyed Ti-4wt%MgB_2

J. A. WILSON*, J. W. STEEDS
H.H. Wills Physics Laboratory, University of Bristol, Bristol, BS8 1TL, UK
E-mail: j.wilson@physics.gla.ac.uk

D. M. J. WILKES, P. S. GOODWIN, C. M. WARD-CLOSE
Structural Materials Centre, DERA Farnborough, Hampshire, GU14 OLX, UK

A Ti-4wt%MgB_2 alloy was produced by mechanical alloying (MA) Ti and MgB_2 powders for 48 hours in a Spex 8000 mill. TEM analysis of the alloy showed it to consist of a nanocrystalline (10–20 nm) Ti matrix, which enclosed 20–300 nm MgB_2 particles. Following heat treatments at 600°C, plate like structures of a previously unknown compound were observed to have extended into the crystals. Convergent beam electron diffraction (CBED) confirmed the new phase to have the same basic arrangement of atom sites as in the NiAs structure. Parallel electron energy loss spectroscopy (PEELS) and energy dispersive X-ray analysis (EDX) measurements identified the elements Ti, Mg and B within these plates. However, the exact proportions of these elements and their distribution within the unit cell could not be determined.

1. Introduction

Titanium and many of its alloys have been used extensively in aerospace applications for their high specific strength, good high temperature performance and corrosion resistance. Lately, the desire to improve aircraft efficiency has led to experimentation with novel light alloys based on titanium. One such alloy which has attracted attention from a number of groups recently is the binary titanium-magnesium system [1–8]. A 15% reduction in weight would be achieved by alloying titanium with 11% magnesium. However, complete mixing of the elements in such a ratio cannot be achieved by conventional casting methods as the boiling point of magnesium (1090°C) lies well below the melting point of titanium (1668°C). In addition to this, the equilibrium solid solubility of magnesium in titanium is only 0.7 at% even at 890°C [5]. This solubility seems surprisingly low given that the elements effectively satisfy three of the four Hume-Rothery criteria: similar atomic radii, identical crystal structure and, similar electronegativities. It is only the difference in valency between the two elements (2 and 4 for magnesium and titanium respectively) which, by the final criterion, prevents significant solid solubility from occurring. For this reason novel processing techniques such as physical vapour deposition (PVD)[1–3] and mechanical alloying (MA)[4–8] have been necessary to produce these materials.

Mechanical alloying is a high energy ball milling process originally developed by Benjamin in 1970 [9] for producing oxide dispersion strengthened nickel based alloys. It has since been found to be an effective means of producing metastable solid solutions in systems such as Ti-Mg. Contamination-free Ti-9wt%Mg solid solutions have been reported (Wilkes *et al.* [6]) and improvements in milling conditions have since led to the production of Ti-21wt%Mg [8]. However, when these powders were heated to the temperatures typically required by conventional powder consolidation techniques, the solutions became unstable with the result that the magnesium segregated to the grain boundaries. Similar instability was observed in the heat-treated PVD Ti-Mg alloys [2]. For this reason, a number of more complex Ti-Mg based alloys were prepared by MA in an attempt to achieve improved thermal stability. The material discussed here is Ti-4wt%MgB_2, which was mechanically alloyed for 48 hours.

2. Experimental details

The titanium and magnesium boride powders were milled under a high purity argon atmosphere for 48 hours using a SPEX 8000 high energy ball mill. The processed powder particles, being approximately spherical and typically 10–50 μm in size, presented very little electron transparent area which could be used in TEM analysis. The powder was therefore cold-pressed uniaxially into discs approximately 20mm in diameter and 0.5 mm thick. Sections of these discs were then broken off and mechanically polished down to ~60 microns before being dimpled to ~30 microns. Both the polishing and dimpling were performed using alcohol based lubricants to avoid any possible reaction between water and any free magnesium which might

* *Present Address:* Department of Physics and Astronomy, University of Glasgow, G12 8QQ, UK.

be present in the sample. Following dimpling, the samples were ion thinned at liquid nitrogen temperatures to electron transparency using a Gatan model 600 dual ion mill. Sections of the cold-pressed discs were also heated to 600°C under vacuum in order to assess the thermal properties of the material.

Basic TEM imaging and convergent beam diffraction (CBED) were carried out using a Philips EM430 transmission electron microscope (TEM) running at 250 kV and operating in microprobe mode. CBED analysis of fine structures was performed using the smallest available spot size and condenser aperture. This produced a probe size of ∼20 nm. The samples were mounted in a double tilt holder and positioned eucentrically in the microscope to facilitate tilting. The vast majority of these crystals were too small and thin to allow simultaneous tilting and viewing of Kikuchi bands with the microscope set up in diffraction mode. Tilting was, therefore, performed in imaging mode using the first tilt direction until the grains became as dark as possible. This indicated that the grain was oriented either near a major zone axis or at least along one of the more prominent Kikuchi bands. The second and first tilts were then used in conjunction with each other to tilt the crystals precisely onto the zone axes. Only the final adjustments near the zone axes could be performed whilst viewing the diffraction pattern.

EDX and Parallel Electron Energy Loss Spectroscopy (PEELS) were performed at 200kV using a Hitachi HF2000 cold field emission TEM fitted with a Gatan Imaging Filter (GIF) and a high take off angle EDX detector. The PEELS images were acquired as gain normalised frames, which both subtracted the CCD's dark background counts and accounted for the sensitivity variations across the CCD. Low loss PEELS images were acquired with a 2.5 eV slit and acquisition times of 0.5–2 seconds. The B-K edge images were acquired using a slit width of 10 eV, and the three window method (as described, for example, by Berger *et al.* [10]) was used to perform background subtraction.

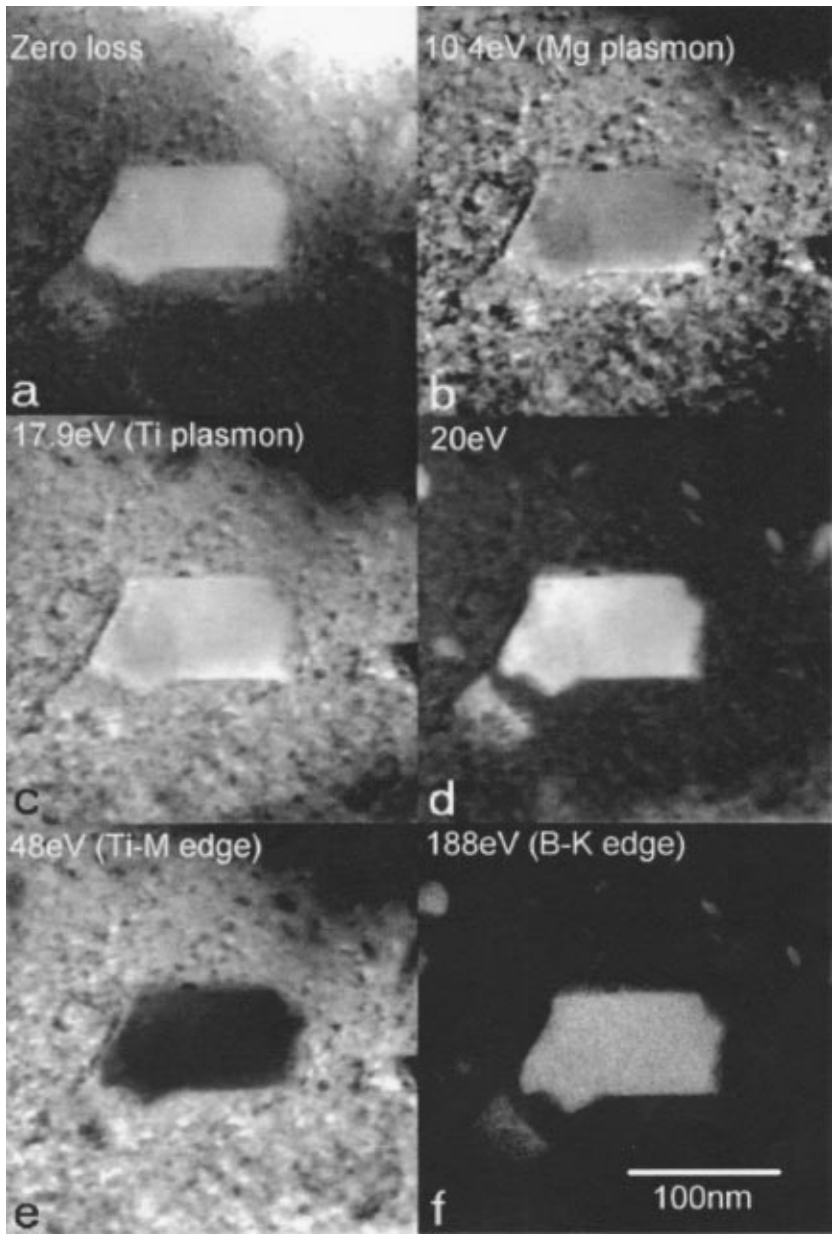

Figure 1 PEELS images of the as-pressed Ti-4%MgB_2 powder showing boride crystals of varying sizes within the Ti matrix.

3. Results

Basic TEM analysis of the cold-pressed material showed it to consist of relatively large grains of magnesium boride (up to 300 nm) surrounded by a nanocrystalline matrix consisting predominantly of very fine grain size (10–20 nm) pure titanium. CBED patterns from the large MgB_2 particles could be indexed to the expected MgB_2 hexagonal crystal structure ($a = 3.08$ Å, $c = 3.52$ Å). EDX traces taken from these crystals showed magnesium to be the dominant peak (core loss X-rays from boron having insufficient energy to penetrate the beryllium window of the detector). Contaminant peaks also resulted from the Ti matrix and Cu slot grid.

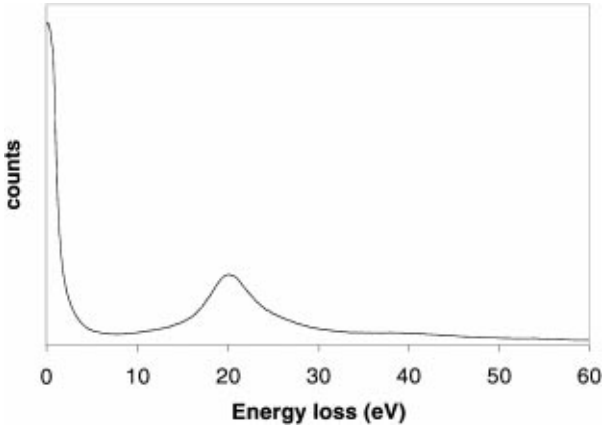

Figure 2 Low loss EELS spectrum from MgB_2 particle within the Ti matrix.

Fig. 1 shows a series of PEELS images of this material. Fig. 1a is the zero loss image. Fig. 1b–d were acquired at 10.4, 17.9 and 20 eV losses which correspond to the bulk plasmon energies for pure crystalline Mg, Ti, and MgB_2 respectively. Fig. 1e corresponds to the Ti-M2,3 edge which has a peak loss at 48 eV, and Fig. 1f to the B-K edge at 188 eV. The large MgB_2 crystals appeared very bright in contrast to the matrix in the image taken at 20 eV loss. Fig. 2 provides a low loss EELS spectrum from one of the large boride crystals. The spectrum shows a broad plasmon edge

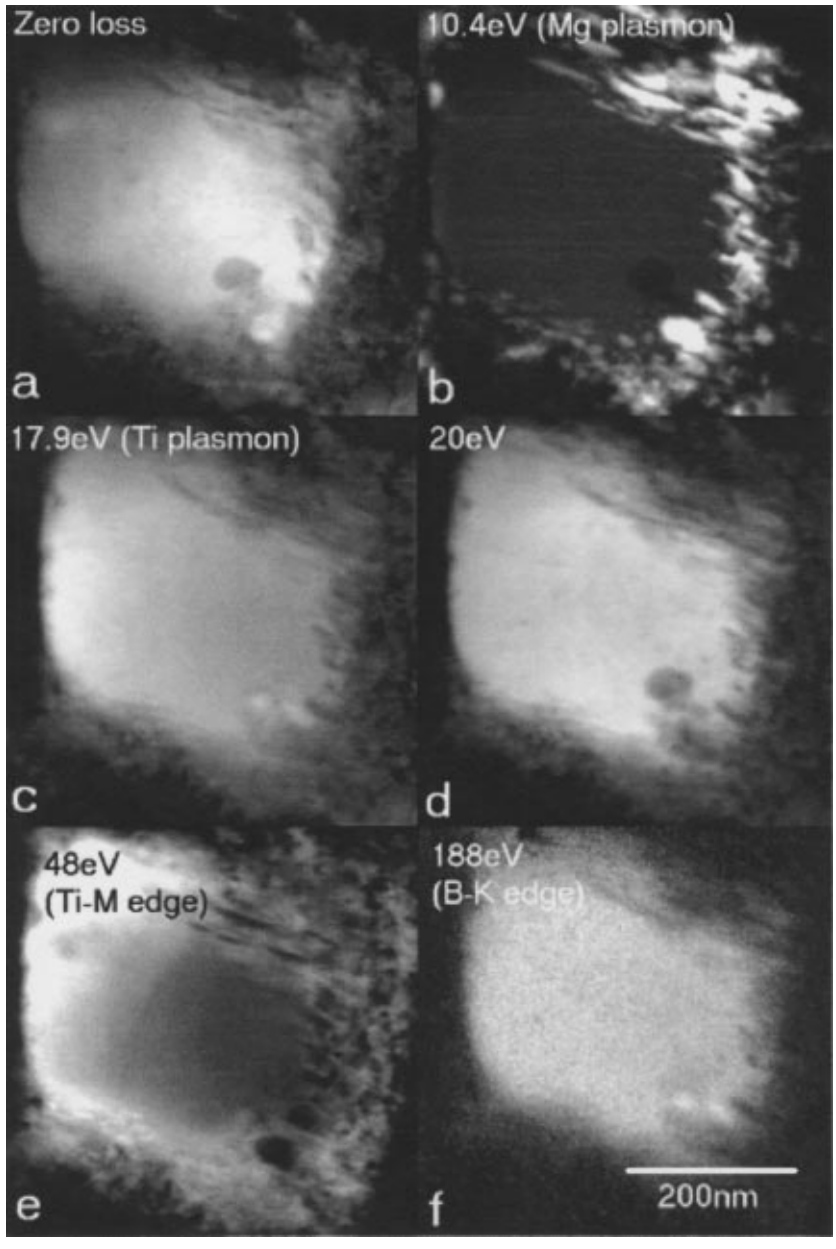

Figure 3 PEELS images of a partially reacted MgB_2 particle in a sample of Ti-4%MgB_2 following heating at 600°C for 30 minutes.

peaked at 20 eV, which we conclude to be the MgB_2 bulk plasmon. In addition to the large crystals, a number of smaller fragments of MgB_2 down to 20 nm in size, which were not easily discernible under normal imaging conditions, were also visible at this energy. The broadness of the MgB_2 bulk plasmon peak explains the relative brightness of the large crystal in the Ti plasmon image acquired at 17.9 eV. An image acquired with a 2.5 eV slit at 17.9 eV energy loss will include a large proportion of the intensity from the MgB_2 plasmon. The B-K edge core loss map in Fig. 1f confirms the presence of boron in both the large and small crystals which were visible at 20 eV. Comparison of this image with the Ti-M edge image shows no evidence of significant interdiffusion of Ti and B atoms at the grain boundaries. The nanocrystalline matrix surrounding the boride particles shows very little variation in contrast when viewed at the various energy losses which confirms it to be predominantly single phase Ti with no free Mg being present.

The material was then heat treated at 600°C for 30 minutes under a vacuum of $\sim 10^{-5}$ torr. The effects of the high temperature anneal on the microstructure were immediately apparent under normal TEM imaging conditions. A fine plate-like structure was observed at the periphery of the boride crystals when they were viewed at orientations perpendicular to the *c*-axis. The plates were typically 20 nm wide and oriented parallel to the longer sides of the crystals, which was generally perpendicular to the direction of the *c*-axis. Fig. 3a–f are a set of PEELS images of one of the reacted crystals. The centre of the boride crystal shows the same variation in intensity with energy loss that was observed in the unheated material. EELS spectra, EDX spectra and diffraction patterns acquired from the centre of the crystal all confirmed it to be unreacted MgB_2. The plate-like structure around the edges of the grains appeared to contain at least two different phases. The first phase appeared bright in the image acquired at 10.4 eV and dark at the other energy losses suggesting that it might be free Mg. The second type of area in between these columns tended to show similar imaging characteristics to the MgB_2 in the centre of the crystals.

The small area of reacted material around these crystals made a thorough analysis using CBED and EELS essentially impossible. For this reason, a longer heat treatment of 3 hrs at 600°C was performed in order to provide a larger reacted area. Following this anneal, the reacted structure was usually found to extend through the entirety of the boride crystals. In the largest crystals, an unreacted core was still visible, but in all cases, the reaction was much nearer to completion.

CBED patterns obtained from the central unreacted cores showed the expected MgB_2 $\langle 1,0,-1,0\rangle$ and $\langle 1,-2,1,0\rangle$ zone axis patterns. The basic MgB_2 reflections would remain visible as the beam was moved towards the particle periphery, but extra spots would then appear in between them. The number of extra reflections was found to vary somewhat, but a few of the more prominent examples were almost always present. The rows corresponding to higher l values clearly showed a definite departure from linearity. Figs 4a and 5a respectively show typical $\langle 1,0,-1,0\rangle$ and $\langle 1,-2,1,0\rangle$ zone axis patterns from the plate-like regions. It was found that these patterns could be indexed very effectively in terms of the original MgB_2 hexagonal lattice together with a second hexagonal lattice with parameters $a = 3.11$ Å and $c = 5.17$ Å. The lattices are essentially aligned with each other, and when crystal orientation was favourable, a tilt of 60° between successive $\langle 1,0,-1,0\rangle$ or $\langle 1,-2,1,0\rangle$ produced identical patterns. Whilst tilting about the *c* axis the boundaries between the columns remained clearly distinct, whereas tilting perpendicular to this direction would significantly reduce the boundary contrast. This confirmed that the two phases visible in the images existed in plate-like structures which extended a significant depth through the sample.

No compound with an elemental composition based on Ti/Mg/B and with these lattice parameters had previously been documented, which suggests that the reaction involved the formation of a new phase. Completely

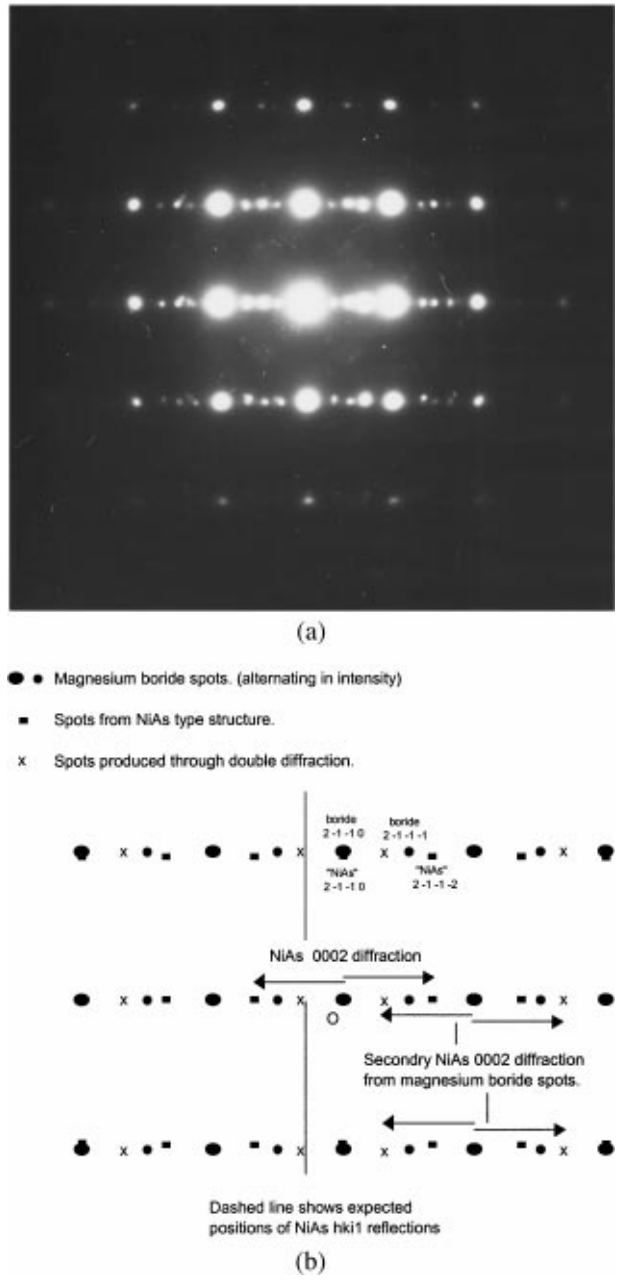

Figure 4 (a&b) Real and schematic [0,−1,1,0] zone axis patterns from a reacted portion of the boride crystals.

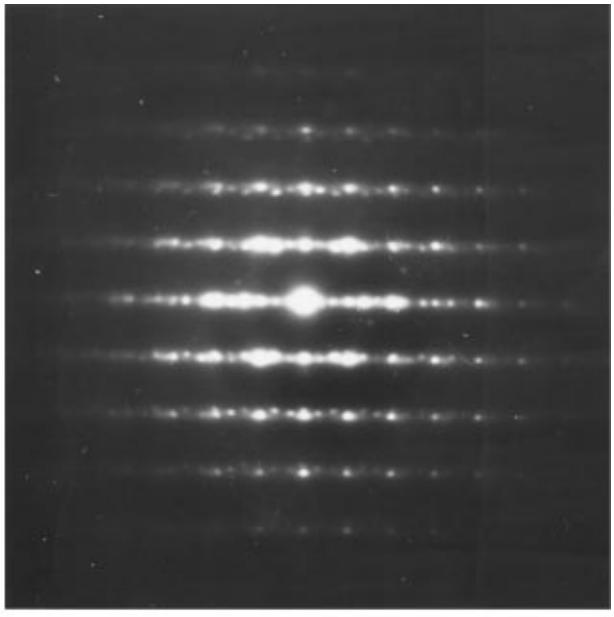

(a)

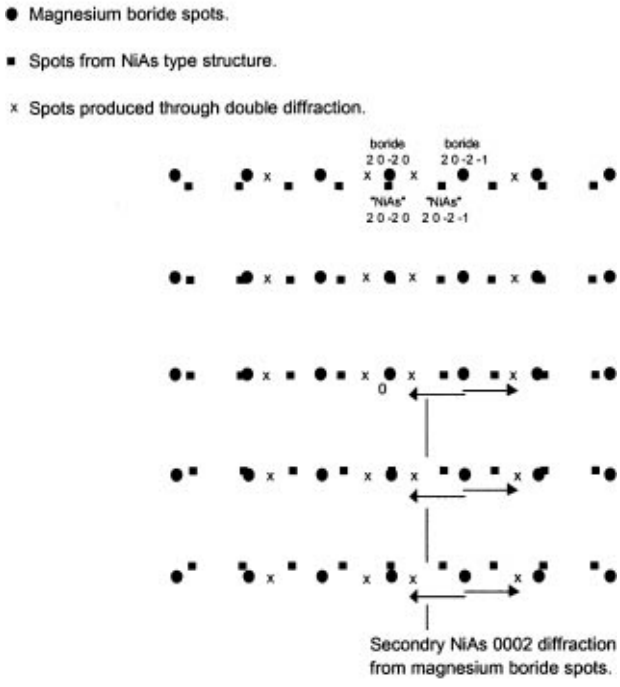

(b)

Figure 5 (a&b) Real and schematic [1,−2,1,0] zone axis patterns from the reacted boride crystals.

new arrangements of atom sites in cells of this size are very rarely encountered so a hypothetical Ti-Mg-B crystal structure was based around the most frequently occurring atomic arrangement with similar cell constants. Using determinative tables, it was found that the c:a ratio of the new structure compared very favourably with that of the NiAs structure. A possible hypothetical structure based on the NiAs atom arrangement, which could readily be explained in terms of intergrowth of Ti into the MgB_2 lattice, was the compound $TiMgB_2$. In this arrangement, the boron atoms occupied the As sites (1/3, 2/3, 1/4 and 2/3, 1/3, 3/4) and alternate Ti and Mg atoms occupied the Ni sites (0,0,0 and 0,0,1/2). The variations which were observed between $\langle 1,0,-1,0\rangle$ and $\langle 1,-2,-1,0\rangle$ patterns could be explained in terms of varying degrees of double diffraction occurring between the two hexagonal lattices. The patterns provided in Figs 4a & 5a are explained schematically in Figs 4b and 5b, where different markers have been used for spots resulting from the MgB_2 diffraction, diffraction from the new structure and double diffraction events between the two structures. A structure factor calculation was performed for the proposed Ti-Mg-B structure and the resulting values for each reflection were compared with the observed diffraction patterns. A degree of consistency was found between the intensities of the reflections from the new phase and the calculated structure factor values. The incidences of double diffraction could also be accounted for in terms of the structure factors for both phases.

A schematic pattern for the [0,−1,1,0] axis is given in Fig. 4b. The principal structural effect on the brightness of the NiAs type reflections at this axis is the complete absence of reflections of the type $(2h,-h,-h,2n+1)$ where n is an integer. The absence of reflections such as (0,0,0,1) is not consistent with a strictly alternating arrangement of Mg and Ti atoms. In this case the intensity of the (0,0,0,1) would be significant and related to

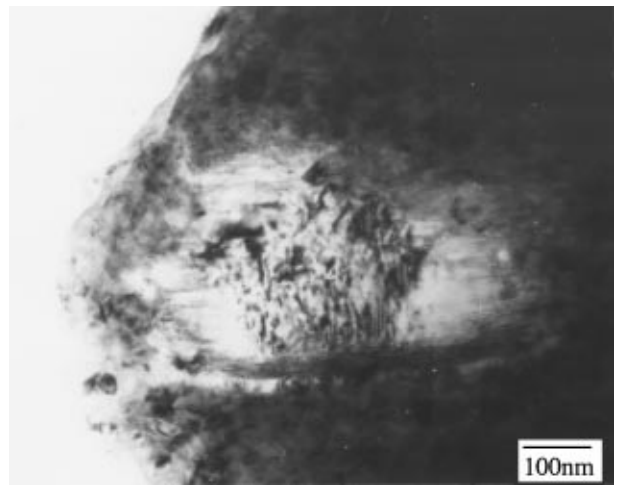

(a)

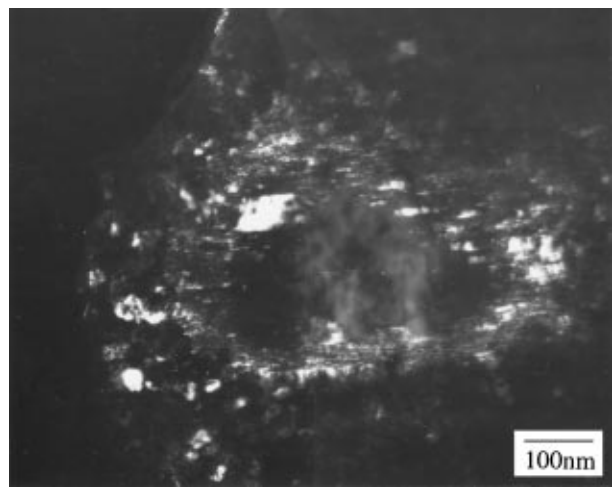

(b)

Figure 6 (a) Bright field image of a MgB_2 crystal at [1,0,−1,0] orientation in the alloy heated for 30 minutes at 600°C. (b) Dark field image of the same crystal taken using the (0,0,0,2) spot from the "NiAs" type structure.

the difference between the atomic scattering factors of Ti and Mg. The absence of these reflections could, however, be explained if the Ti and Mg atoms randomly occupied these sites over an extended spatial range. The principal incidences of double diffraction visible at this axis comprise MgB_2 $\{h,k,i,2n\}$(the brighter MgB_2 spots) followed by "NiAs" type $(0,0,0,\pm 2)$.

At the $[1,-2,1,0]$ axis, structure factor calculations predicted a relatively low intensity for "NiAs" type reflections of the type $\{h,0,-h,l\}$ where h is a multiple of three and l is odd. This is consistent with Fig. 5a, where reflections of the type $\{1,0,-1,l\}$ and $\{2,0,-2,l\}$ in the NiAs structure are present for all values of l, whereas reflections of the type $\{3,0,-3,l\}$ are barely visible for l odd. The $\{0,0,0,l\}$ reflections were also missing for l odd. This is shown schematically in Fig. 5b but is not clear in the actual diffraction pattern due to overexposure in this region. However, the alternating brightness of these reflections may be inferred from the strong double diffraction incidences observed in this pattern. These result from MgB_2 diffraction followed by $\{0,0,0,2\}$ rather than $\{0,0,0,1\}$ NiAs type diffraction as indicated in Fig. 5b.

On the basis of these results the most probable structure for this reacted phase is based on the NiAs structure with B atoms occupying the As sites and Ti and Mg atoms randomly occupying the Ni sites. In fact it is quite possible that the relative proportions of Ti and Mg within the structure may vary from point to point along the plates.

The relative distribution of the two phases was mapped by taking dark-field images using the first $(0,0,0,l)$ spot of the new reacted phase. A bright field image of a boride crystal in the 30 minute heat treated material together with (0,0,0,2) dark field image are given in Fig. 6. The dark field image shows alternately bright and dark columns similar to those observed in the 10.4 eV PEELS image in Fig. 3. The dark field image also demonstrates the very fine scale on which the reaction can take place; the two fine bright lines in the centre of the crystal are less than 5 nm across.

EDX and EELS were employed to assess qualitatively the distribution of elements within the reacted sections of the columnar structure. Quantitative work was not possible due to large thickness variations, grain overlap and fine scale composition variations. Fig. 7 gives PEELS images of a portion of a reacted crystal taken at zero loss, 10.4 eV and 20 eV. Both the reacted regions of the periphery and the central core are visible. Three points: A, B and C were selected for EDX and EELS analysis. A circular aperture which selected an

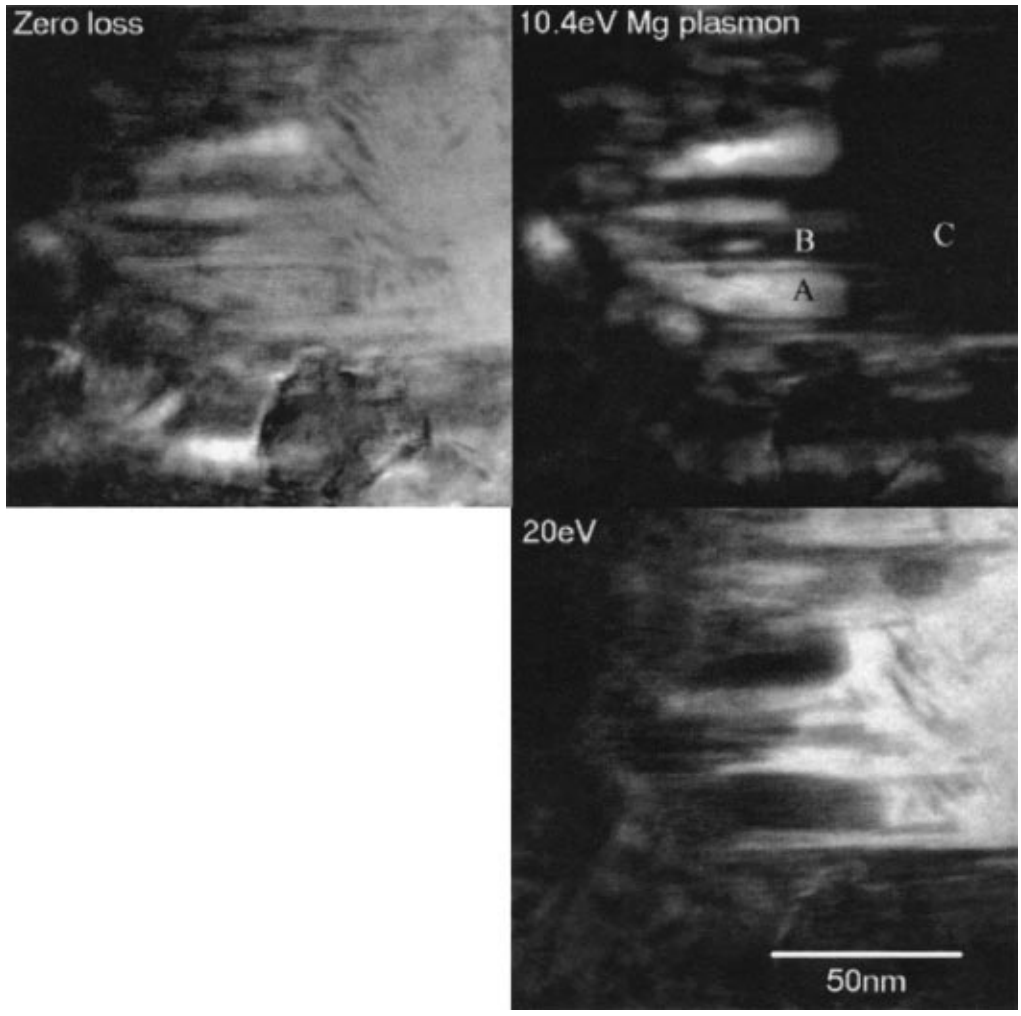

Figure 7 PEELS images of a portion of a partially reacted crystal in the material heat-treated for 30 minutes. EELS and EDX spectra were acquired from the points A, B and C.

area ~10 nm in diameter was inserted into the image plane of the spectrometer at the positions marked A, B and C in Fig. 7 and EELS spectra were acquired from each of these selections.

The spectrum taken from the central core at point C was essentially identical to the unreacted MgB_2 spectrum in Fig. 2. Profiles of the low-loss spectra from the regions A & B are displayed in Fig. 8a and b. The profile of the spectrum from point B shows a principal plasmon peak at 20 eV which is, again, similar to that of the unreacted MgB_2. The spectrum profile from point A has its highest peak at 10.5 eV which is almost the same energy as the Mg plasmon peak. There is significant cross contamination between these two profiles as a result of averaging over an extended area and also as a result of composition variations with depth through the sample.

Portions of the EELS spectra at higher energy losses are given in Fig. 8c and d. The relative intensity of the B-K edge in the EELS spectrum from point B was similar to that observed in the spectrum from the unreacted boride in the centre of the crystal, although a small Ti peak, almost certainly resulting from contamination from the adjacent plates, was visible. In the spectrum from point A the relative intensity of the boron peak was considerably reduced and a very prominent Ti-K edge peaked at 470 eV was visible confirming that a significant amount of Ti had permeated this material.

EDX traces from the points A and B are given in Fig. 9a and b. The spectra were both recorded with an acquisition time of 60 seconds. There is a significant contaminant copper peak due to the proximity of the copper slot grid upon which the specimen was mounted. The Mg and Ti peak heights at point B were found to be approximately the same as those in a trace taken at C from the unreacted core. Ti was a major contaminant in spectra acquired from MgB_2 particles in the unheated sample and so the presence of this peak does not necessarily indicate that reaction has taken place at these positions. However, a significant jump in the relative height of the Ti peak is noticeable in the spectrum taken from point A.

The EDX and EELS results confirm that the plasmon peak observed at 10.5 eV in the EELS spectrum from region A is not due to pure Mg and explains the absence of Mg spots in diffraction patterns acquired at the edges of the MgB_2 crystals. The peripheral portion of the crystal consists of plates alternating between MgB_2 and the new Ti-Mg-B phase. The fact that the plates of the new Ti containing phase are relatively dark in the Ti-M image at first seems surprising. However, it must be remembered that there is significant background from other peaks at this energy, particularly the MgB_2 second plasmon at 40 eV. In addition to this, the proposed crystal structure for these regions contains both Mg and B atoms which will reduce the relative intensity of the Ti core loss signal here. At 48 eV there is likely only to be very low plasmon intensity from the new phase as this would require a high proportion of four and five fold multiple plasmon excitations.

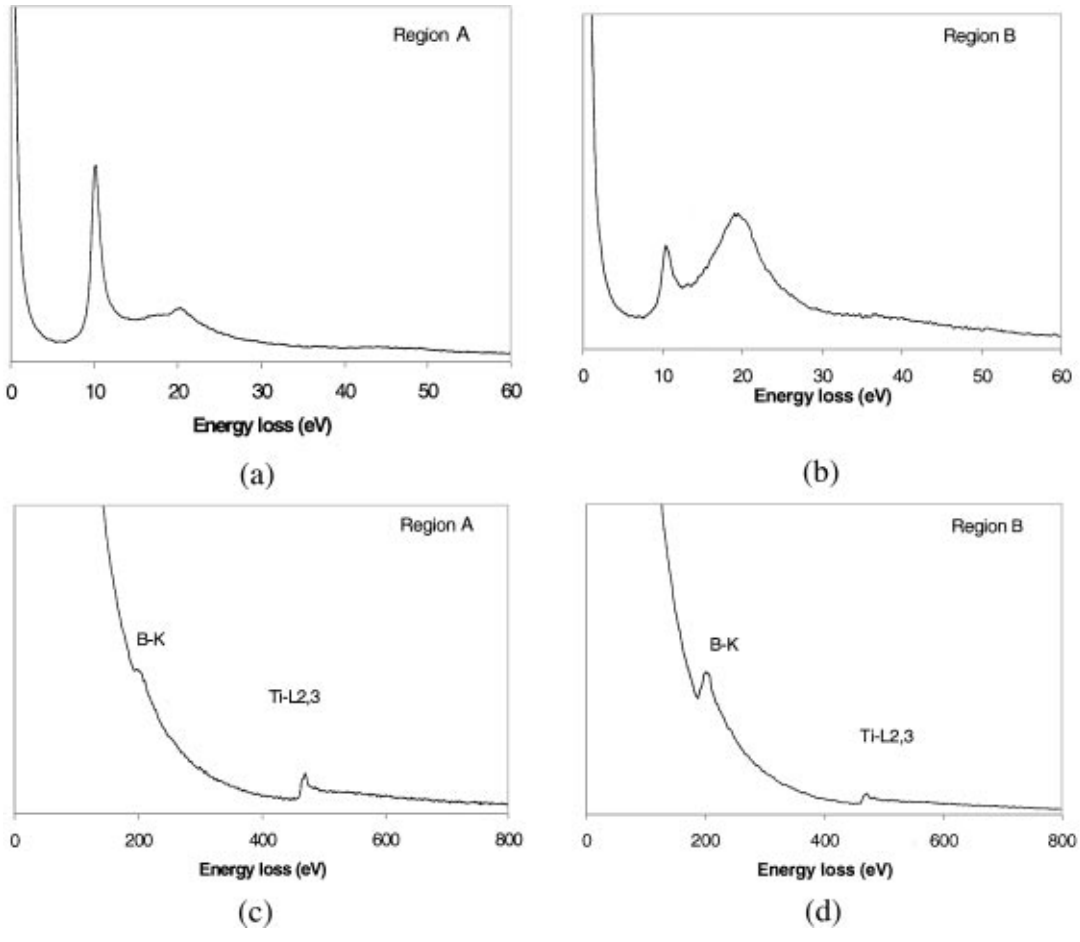

Figure 8 (a&b) Low loss EELS spectra from points A and B in Fig. 7. (c&d) Higher energy loss regions of the spectra given in a&b.

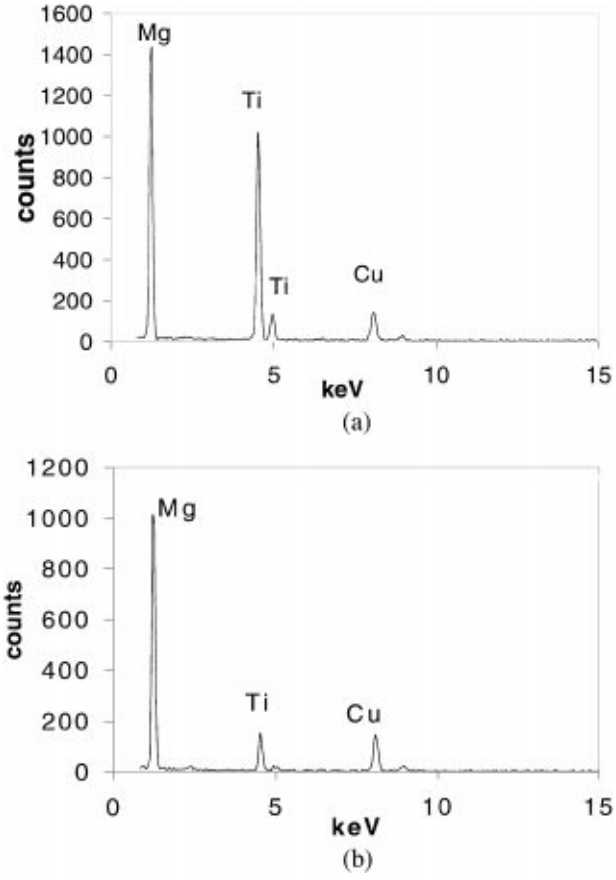

Figure 9 (a&b) EDX spectra from the points A and B in Fig. 7.

The fact that a significant amount of Ti has invaded the large MgB_2 grains to produce the observed plate like structures is, perhaps, not surprising when one considers the relative enthalpies of formation of Mg and Ti borides. At 900 K the enthalpy of formation of MgB_2 is −97 kj/Mol whereas that of TiB_2 is −326 kJ/Mol [11]. Due to the very fine scale of the reaction it was, however, not possible to determine exactly how much Ti was entering the crystal or how quickly the process was occurring. Examination of the Ti matrix region and the smaller boride crystals suggested some Mg was displaced to the matrix as the Ti reacted with the crystal.

PEELS images of the matrix material surrounding the larger reacted crystals are provided in Fig. 10. There are numerous 10–50 nm bright regions visible in the 10.4 eV loss image. The figures are reminiscent of those of heat treated binary Ti-Mg alloys produced by physical vapour deposition (PVD) or MA [12, 13]. However, this image is not sufficient in itself to prove that pure Mg is present at the grain boundaries as it has been shown that the reacted portions of the large boride grains also appear bright at 10.4 eV, despite having a different crystal structure. It is also important to note that there were numerous small fragments of MgB_2 observed in the unheated material, which were similar in size to the bright areas in Fig. 10.

Core loss spectra from these regions frequently did not show a B-K edge at 200 eV but a Ti edge was visible. When the B-K edge was present it was very

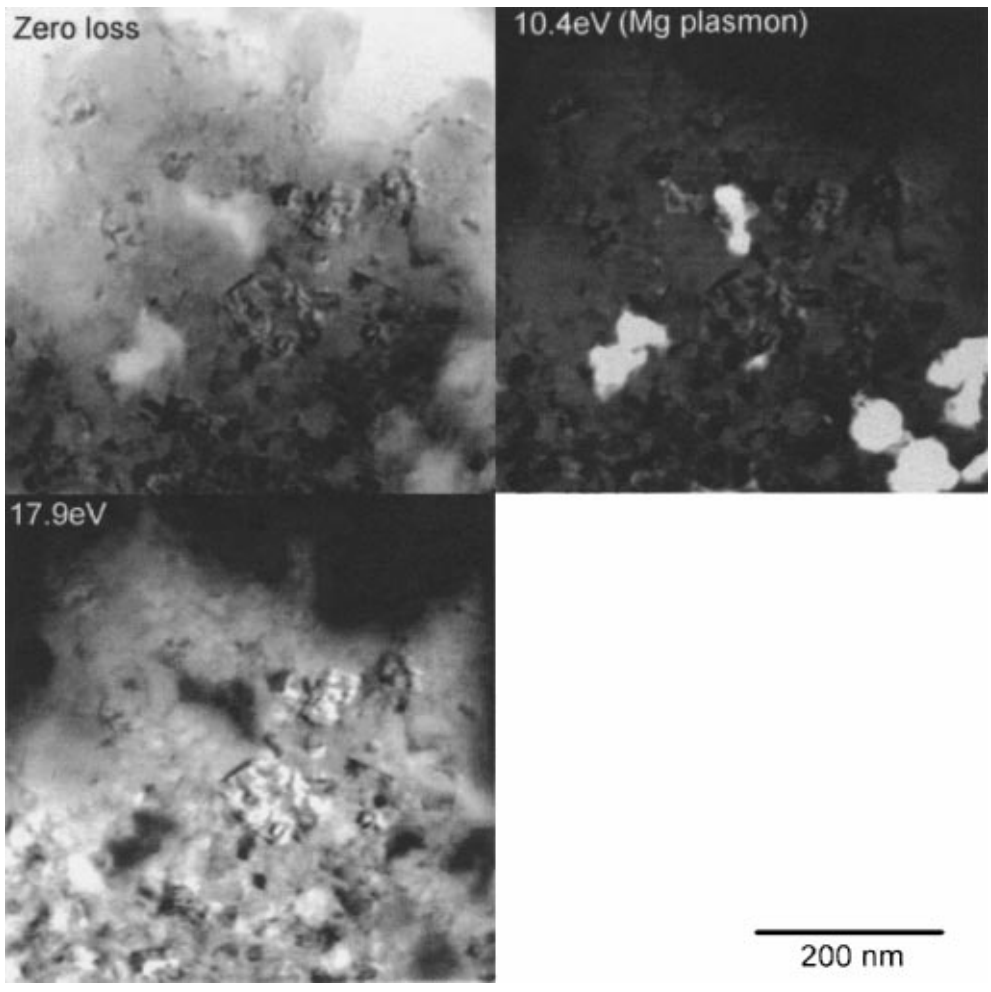

Figure 10 PEELS images of the matrix region of the heat-treated Ti-4%MgB_2 away from any large boride crystals.

low compared to the background and the higher energy Ti edge. The Ti edges observed in these spectra are predominantly caused by contamination and overlap by the Ti matrix and do not necessarily indicate that these regions are the reacted Ti-Mg-B rather than pure Mg.

The presence of regions of almost pure Mg in the matrix was, however, confirmed by taking SAD ring patterns from areas of the sample which did not contain any of the larger boride crystals. A significant number of spots corresponding to both Mg and the new reacted phase were observed. This demonstrates that some Mg tends to be displaced from the boride crystals as the Ti reacts with them. Thus, bright regions of the matrix in the 10.4 eV loss images could represent either pure Mg or the reacted Ti-Mg-B phase.

4. Conclusions

Mechanical alloying Ti with 4 wt% MgB_2 powder in a Spex mill for a period of 48 hrs resulted in a fine grain size ($\sim$20 nm) Ti matrix containing MgB_2 crystals between 20 and 300 nm in size. Upon heat treatment at 600°C for 30 mins, a reaction between the matrix and the boride crystals took place, which resulted in the formation of a new Ti-Mg-B hexagonal phase with the same basic arrangement of atomic positions as the NiAs structure. Due to the thickness variations in the sample, phase overlap and fine structures, the respective abundances of the three elements in the cell could not precisely be determined through EELS or EDX methods. However, it seems likely that there is some variation of the local composition along the plates as Ti invades the boride crystals and some Mg is displaced to the Ti-matrix. The use of low angle ion-thinning techniques on these samples might produce thinner and flatter reacted boride crystals thereby allowing semi-quantitative EELS and EDX analyses to be performed on the new phase.

The fact that a significant amount of Mg is displaced from the boride crystals to the Ti grain boundaries suggests that this alloy, if consolidated, may suffer from similar deficiencies in mechanical performance to the Ti-Mg binary system. However, the rate of reaction is relatively slow, as can be seen from the differences between the 30 minute and three hour heat treatments. If powder consolidation could be achieved in shorter times, a relatively light dispersion strengthened alloy with good mechanical properties might result.

Acknowledgements

The authors wish to thank the Engineering and Physical Sciences Research Council (EPSRC) and the Defence Evaluation and Research Agency (DERA) for their support of this work

References

1. C. M. WARD-CLOSE and P. G. PARTRIDGE, *Mater. Lett.* **11** (1991) 295.
2. G. LU, P. G. PARTRIDGE, J. W. STEEDS and C. M. WARD-CLOSE, *J. Mat. Sci.* **31** (1996) 867.
3. J. G. ZHENG, P. G. PARTRIDGE, J. W. STEEDS, D. M. J. WILKES and C. M. WARD-CLOSE, *ibid.* **32** (1997) 3089.
4. C. SURYANARAYANA and F. H. FROES, *J. Mater. Res.* **5** (1990) 1880.
5. E. ZHOU, C. SURYANARAYANA and F. H. FROES, *Mater. Lett.* **23** (1995) 27.
6. D. M. J. WILKES, P. S. GOODWIN, C. M. WARD-CLOSE, K. BAGNALL and J. W. STEEDS, *ibid.* **27** (1996) 47.
7. M. HIDA, K. ASAI, T. TAKEMOTO and A. SAKAKIBARA, *Materials Transactions (JIM)* **37** (1996) 1679.
8. D. M. J. WILKES, P. S. GOODWIN and C. M. WARD-CLOSE, in "Metastable Phases & Microstructures," MRS 1996, Vol. 400, edited by R. Bormann *et al.* (MRS 1996) p. 267.
9. J. S. BENJAMIN, *Metall. Trans.* **1** (1970) 2493.
10. A. BERGER, J. MAYER and H. KOHL, *Ultramicroscopy* **55** (1994) 101.
11. I. BARIN, "Thermochemical data of pure substances" 2nd ed (VCH, New York, 1993).
12. K. BAGNALL, PhD. Thesis 1996, University of Bristol.
13. J. A. WILSON, PhD. Thesis 1998, University of Bristol.

Received 10 December 1999
and accepted 24 May 2000